Chapter 8

The Adequate Classification of Form in Pathology

We pathologists are engaged in making diagnosis of diseases by examining the form of cells, tissues and organs microscopically and macroscopically. During the past 20 years, various technique including immunohistochemistry and molecular biology has been introduced, greatly contributing to improved accuracy of diagnosis. To the credit of these methods is *reproducibility* with which we have become capable to confirm the presence of specific molecules in the cells or tissues. But even now, morphology, the study of form, remains to be the core of what pathologists are required to perform, train themselves in, and develop. The importance of morphology in clinical pathology will not be reduced even in the future. However, pathologists over the world do not always appear to have managed to improve the accuracy and reproducibility of morphological diagnosis.

Normal, cancer and intermediate cells (Fig. 8-1)

Look at Fig. 8-1. Imagine that the cell in the upper left part of the figure is a normal cell, and that in the right upper, a carcinoma cell. The difference is definable in purely morphological terms: a carcinoma cell is characterized with what is called a severe cellular atypia. However, we so often experience cells with a form quite intermediate between the normal and carcinoma, as shown in the lower part of the figure. Already in the foregoing chapters we have seen such quasi-carcinoma cells in adenomas of the colon and stomach, and in dysplasia of the hepatohilar bile ducts. When faced this sort of cells, sometimes pathologists may waver in determining the diagnosis, and visit their colleagues to discuss. It often happens however that they all fail to reach a conclusion, with different opinions not tending to converge. What should be done on such an occasion? Pathologists then seem likely to think that it may be the one who has the largest experience that could deliver the most correct diagnosis.

I do not think this tradition should be changed. We have to bear social responsibilities, and often it is necessary to have our diagnosis strengthened with experience as much as possible. Only from a scientific viewpoint, however, there may be problems if this sort of decision-making covers the entire aspect of pathological research. Science requires a decision to be a reproducible one, and reproducibility cannot be ensured by personal experience alone. I have to confess that even after having been engaged for many years in the practice of diagnostic pathology, it remains beyond my power to reproduce 100% of diagnosis I made in the past. Much less, among different pathologists who have their own standard of judgment based upon their experience, and it seems almost a daunting task to bring their personal standards to a common

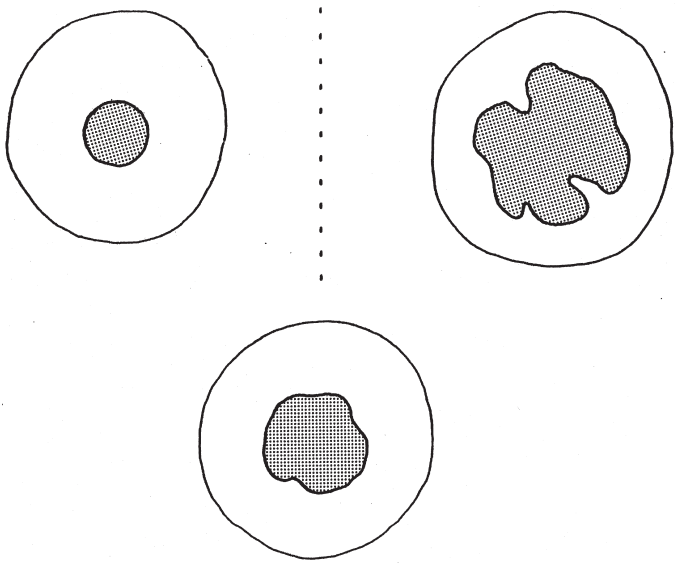

Fig. 8-1. The difference of cancer cell (upper right) from normal cell (upper left) is apparent, but pathologists often encounter cells that assume quite an intermediate form (lower).

level. How to find a solution? Obviously, this requires us to introduce some methods with which to deal with various forms in an objective way. And objectivity can be attained only by introducing quantitative way of thinking into the domain of morphology.

In the following, attempts will be shown to establish a reproducible classification of cellular or tissue changes, mostly led by R. Chiba of our team. Making a morphological diagnosis of an object is, after all, equivalent to deciding, into which of the categories, the object in question is to be classified.

What is classifiability? (Fig. 8-2)

A question has to be answered. Whether or not the disease in question is classifiable at all, and if it is, how to classify. Let us assume in Fig. 8-2 that a large number of subjects were examined for a certain property x, for example, the mean blood pressure. Classification of subjects into two or more groups with regard to x may be justified when, and only when, we have a multimodal distribution as in the upper figure. If tendency to separate did not prove to exist as in the lower, what one can do is only to divide the population in an arbitrary way: at the peak into two groups (1), or into three groups (2) at the levels of plus and minus standard deviation, and so forth. Apparently, this means that the population has been non-classifiable in the first place. Although classification has been and remains the most widely used method of study in pathology, this question of classifiability has never been examined.

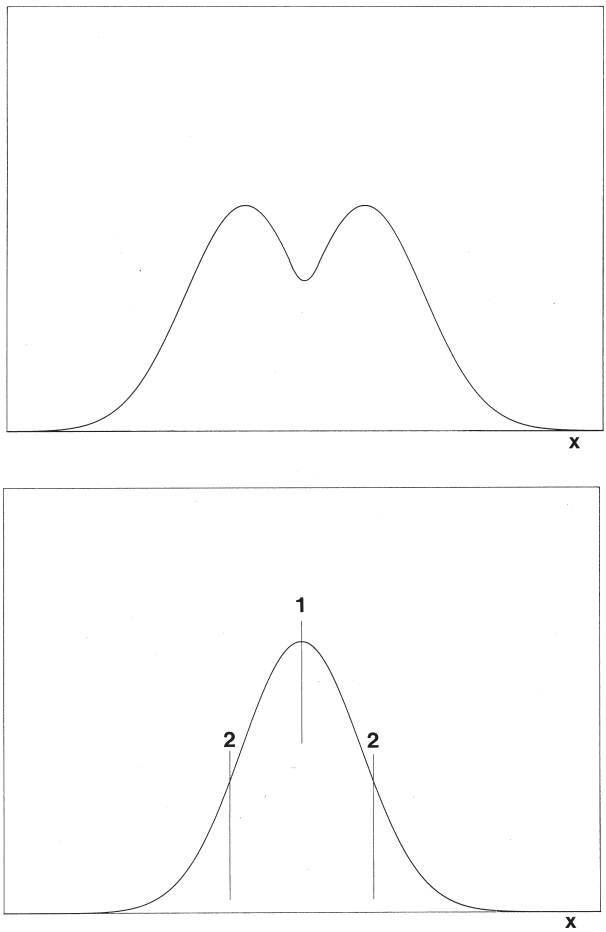

Fig. 8-2. The classifiability with regard to a single property *x*. The subjects are classifiable into groups when, and only when, multimodal distribution was proved as in the upper figure. When the distribution fails to separate as in the lower, the subjects have to be assumed non-classifiable. Reproduced from Chiba and Takahashi: Pathol Int (1994) 44: pp. 672.

a) Adequate classification of liver cirrhosis

Two cirrhoses with different patterns (Fig. 8-3)

Let us begin with the computerized classification of cirrhosis performed by Chiba and Takahashi (1994a,b). Of the two cirrhotic livers exhibited in Fig. 8-3, the left corresponds to Type A and the right to Type B, according to Nagayo's classification (1914) widely used in Japan. In Gall's classification (1960), the former may be expressed as the postnecrotic and the latter, the posthepatitic type.

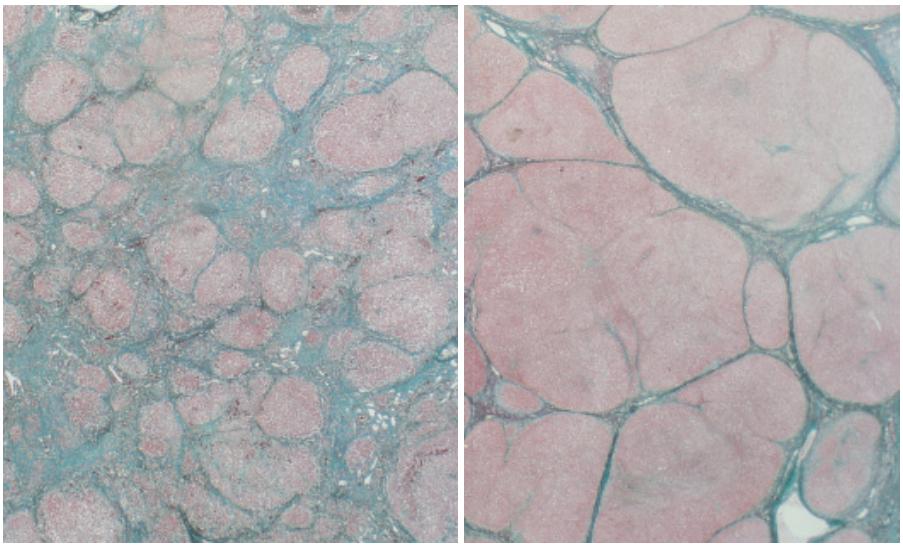

Fig. 8-3. Two cases of cirrhosis with different microscopic pattern. Left: Type A of Nagayo's classification, or postnecrotic type of Gall's, with small nodules and broad interstitial zones. Right: Type B, or posthepatitic type, with coarse nodules and thin, membranous interstitium. Elastica-Goldner stain.

The rationale of classification involving multiple factors of form (Fig. 8-4)

One of the difficulties inherent in the examination of classifiability for lesions like cirrhosis is that the microscopic pattern usually comprises several factors of form instead of a single factor x. As will be shown, in our attempt at computerized classification of cirrhosis, the morphological feature in each case was reduced into a combination of four parameter values. In another series of attempts at classifying carcinomatous and dysplastic cells, we used twelve parameters. Figure 8-4 is a schema explaining the rationale for multiparameter classification, taking as an example the simplest case of two parameters.

Suppose we have five patients, in whom we measured features x and y. The result is depicted in a scatter diagram in the left part of the figure. If we are dealing with cirrhotic livers, then for example x could be the mean radius of nodules and y, the mean thickness of the interstitial septa. At a glance, we immediately realize that in the figure, Cases 1, 2 and 3 form a group or a cluster, whereas Cases 4 and 5 form another. What makes us recognize this grouping? To conclude, it is the difference in the distances among the five cases.

Imagine that the distance was calculated for all possible pairs among the cases in a "round robin." Here we have five cases and consequently, there are (${}_5C_2$=) 10 pairs. The Euclidean distance between Case i and Case j, if written as $d(i, j)$, is defined on the xy-plane as

$$d^2(i, j) = (x_i - x_j)^2 + (y_i - y_j)^2.$$

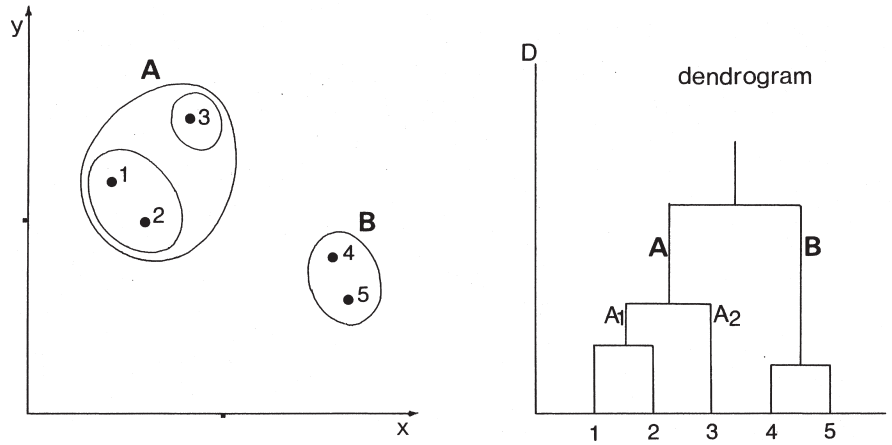

Fig. 8-4. Rationale of cluster analysis for the classification involving multiple factors of form. The left figure presents a simple example of five cases and with two factors x and y. It is clear by inspection that there are two clusters [Cases 1, 2, 3] and [Cases 4, 5]. This grouping is defined by the between-cases distances (see the text). The right figure is the dendrogram drawn based on the distance analysis. Reproduced from Chiba and Takahashi: Pathol Int (1994) 44: pp. 672.

In the figure, one may realize instantly that the distance between the pair of Cases 4 and 5 is the smallest among the 10 pairs, which means that in this pair, one can find the highest similarity. Accordingly, we put these two cases together into Cluster [4, 5]. Next, we compare among the other pairs and confirm the pair of Cases 1 and 2 to be the next nearest, and define Cluster [1, 2]. Then we examine which of the two clusters is nearer to Case 3, and find that Cluster [1, 2] is the case. Thus, finally, the five cases come to be categorized into either two clusters [1, 2, 3] and [4, 5], or three clusters [1, 2], [3] and [4, 5]. The process is visualized in a dendrogram in the right part of the figure. This is the basic principle of cluster analysis, a technique of multivariate statistics, which allows us to determine an order of hierarchy within a large population according to the grade of similarity among the individuals. In the attempt at quantifying the pattern of cirrhosis, a set of four parameters x, y, z and u were used in expressing the form. Therefore the between-individuals difference was defined as a four-dimensional Euclidean distance, as

$$d^2(i,j) = (x_i - x_j)^2 + (y_i - y_j)^2 + (z_i - z_j)^2 + (u_i - u_j)^2.$$

Of course, a space of more than three dimensions is no longer visible, but the distance is definable in whatever dimensions, at least in mathematical terms. Here it only has to be added that in calculating the between-individuals distance $d(i,j)$ in cirrhosis, standardization is necessary for each parameter with the corresponding variance σ, as

$$d^2(i,j) = (x_i - x_j)^2/\sigma_x^2 + (y_i - y_j)^2/\sigma_y^2 + (z_i - z_j)^2/\sigma_z^2 + (u_i - u_j)^2/\sigma_u^2.$$

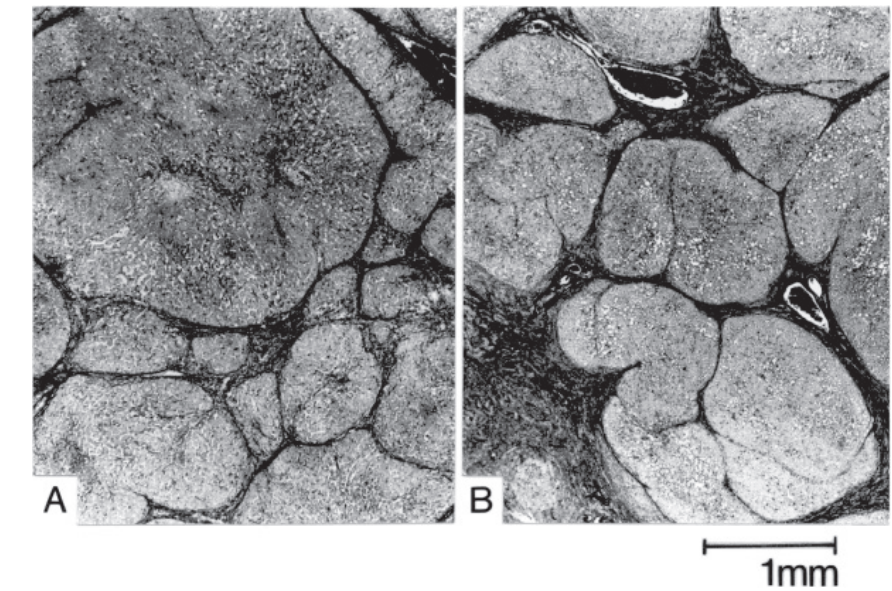

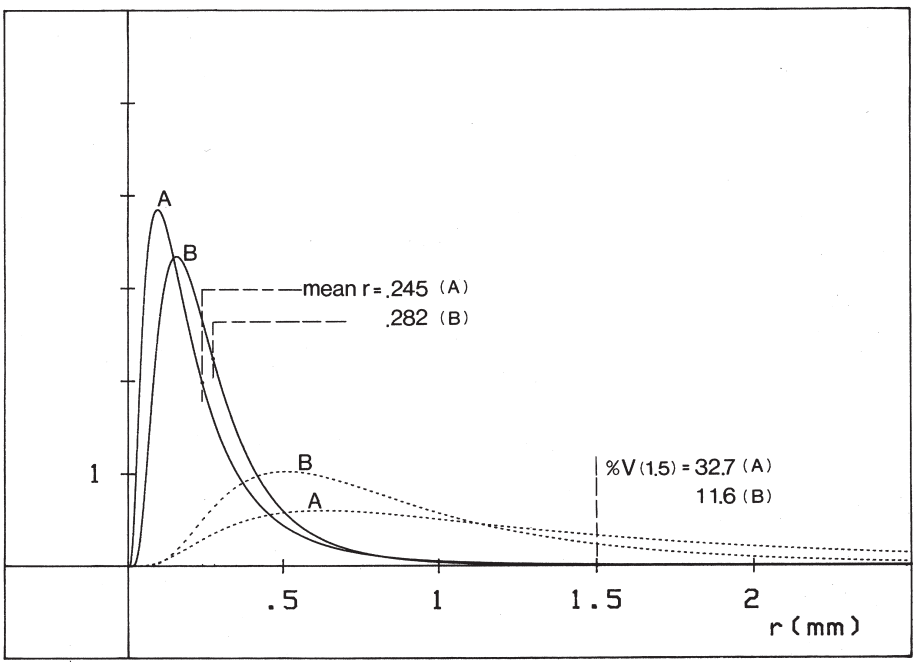

Fig. 8-5. Numerical and volume distribution of nodules in two cirrhoses, Cases A and B. The mean radius in Case B is larger than in Case A, but the numerical curves cross, and in the larger range of *r*, Case A comes higher. This brings about a difference in %V(1.5) which is larger in Case A. The difference in the pattern between Cases A and B is shown in the upper microphotographs, where Case A gives an impression of cirrhosis coarser than Case B. Reproduced from Chiba and Takahashi: Pathol Int (1994) 44: pp. 666.

Of the various methods for defining the distance between clusters, we employed the Ward method (1963) which gave the clearest separation in comparison with other methods of clustering. Computation was performed using a mainframe.

Parameters employed for characterization of cirrhosis (Table 8-1, Fig. 8-5)

In this study, the morphological feature of cirrhotic liver was reduced to four quantities listed in Table 8-1. A total of 70 cirrhotic livers were entered.

The form of cirrhosis was assimilated to the geometric model of dispersed spheres already explained in Chapter 2 where the islets of Langerhans were studied. There, islets were assumed to spheres of various radius *r* dispersed in the space. While Weibull distribution was assumed for the radius of islets, this time the radius *r* of cirrhotic nodules was considered to follow logarithmic normal distribution. In cirrhosis too, as schematized in Chapter 2 (Fig. 2-6), nodules appear in a section as circles of various dimension. If a test line of sufficient length is randomly drawn on the section, it traverses nodules and generates chords of different lengths λ. The length λ was measured under microscope for about 200 consecutive chords. For the rationale of stereological method, see the original articles.

Of the parameters, %V(1.5) means the volume % of nodules larger than 1.5 mm in radius. In Fig. 8-5, volume distribution of nodules (the dotted curves) in two cirrhoses, Cases A and B, is added to the numerical distribution (the solid curves). The mean *r* is 0.245 mm in A and 0.282 mm in B. However, the numerical distribution curves cross, showing that although the mean *r* is larger in Case B, the curve of Case A trails over Case B in the larger range of *r*. This brings about a clearer difference between the two cirrhoses in the volume distribution as shown by %V(1.5). It expresses the share of area under the volume distribution curve in the range of $r \geqq 1.5$ mm, which in Case A is calculated at 32.7%, while it remains 11.6% in Case B. Roughly speaking, a coarsely nodular pattern is represented by a curve trailing far toward the larger *r*, giving a higher %V(1.5); there is no need for the mean *r* also to be large. In fact, the pattern of Case A gives an impression of cirrhosis coarser than Case B, as shown in the b & w pictures.

The thickness of the interstitium *Ds* was defined as a 3-D quantity. For this, the plate model used to determine the thickness of alveolar septa was available without any modification. The model was introduced in Chapter 2 (see Fig. 2-26).

In some cirrhoses, nodules were seemingly well separated in section, while in others they were mutually aggregated. Thus, the degree of nodular separation was

Table 8-1. The four parameters employed for the cluster analysis of cirrhosis. %V(1.5): the volume % to the total of nodules larger than 1.5mm in radius, serving as a parameter of nodular coarseness. *Ds*: the thickness of interstitium defined as a 3-D quantity.

mean *r*:	the mean radius of nodules as assimilated to spheres of various dimension
%V(1.5):	parameter of nodular coarseness, defined by the volume % of nodules larger than 1.5mm in *r* to the total nodular volume
Ds:	the mean 3-D thickness of the interstitium.
ρ_θ:	the grade of nodular separation ($-1.0 \leqq \rho_\theta \leqq +1.0$)

considered to be an important factor of form. To this, ρ_θ defined in Chapter 7 as the index of nodular separation was directly applicable.

Cluster analysis of 70 cirrhoses (Figs. 8-6, 8-7, Table 8-2)

The result of cluster analysis for 70 cirrhotic livers is exhibited in the dendrogram of Fig. 8-6. This is the optimal clustering that satisfies the condition defined above. Of course, the classification thus brought about by computer is reproducible. It is

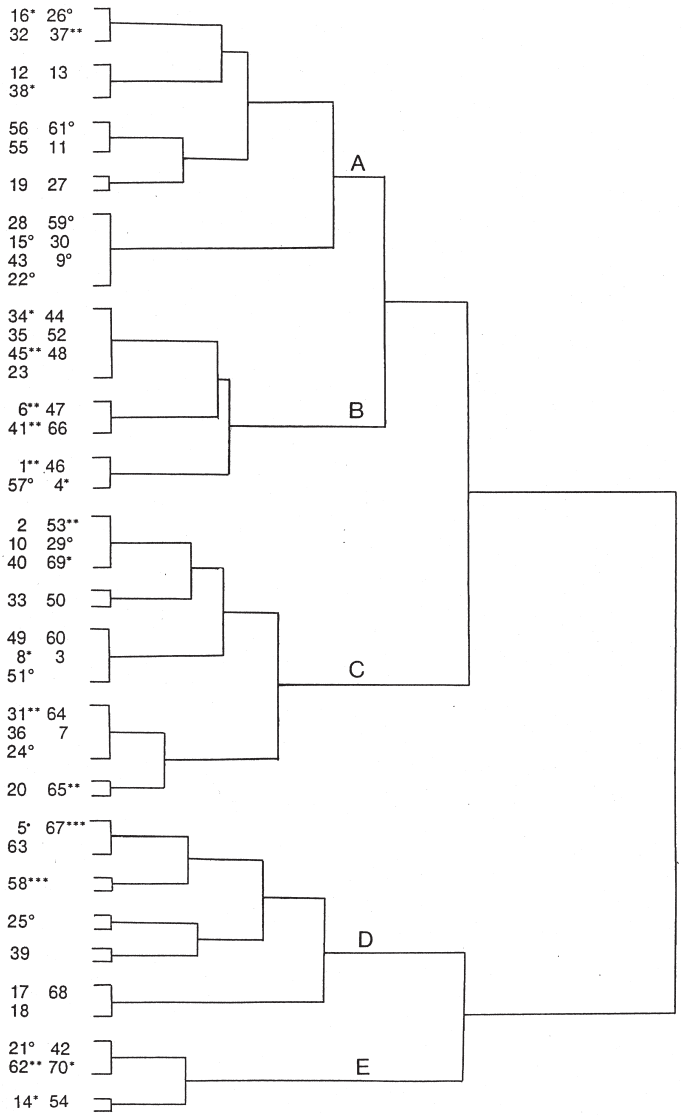

Fig. 8-6. The dendrogram obtained by cluster analysis of 70 cirrhoses. Five clusters, A, B, C, D and E proved to form. Reproduced from Chiba and Takahashi: Pathol Int (1994) 44: pp. 676.

based only upon the form of the objects. In the above process, the objects have assembled or divided themselves only according to their form. We think this can be called the natural classification, discriminating from the conventional, artificial classification.

Five clusters, A, B, C, D and E were obtained. Mean parameter values for each cluster are listed in Table 8-2. Shown in Fig. 8-7 are the microscopic appearances, each of which seems representing the cluster it belongs to, with the parameter values closest to the cluster mean. In Cluster A, the pattern is characterized by membranous interstitium that is the thinnest of all, a mean nodular radius that is also small, and a remarkable fineness of pattern as expressed by a small %V(1.5). A moderately high ρ_θ implies that the nodules are well separated. The pattern may be a typical feature of nutritional (or septal) cirrhosis of Gall's classification. Cluster B also has relatively thin septa, while in this cluster the nodules are much larger as revealed by both the mean r and %V(1.5). This combination of coarse nodules and thin septa is considered to reflect the pattern of posthepatitic cirrhosis of Gall, or Type B cirrhosis of Nagayo. In Cluster C, the nodules are small with both the mean r and %V(1.5) being the lowest of the five clusters, while the septa are thick and the nodules are well separated. Apparently, this describes the pattern of postnecrotic type, or Nagayo's Type A. Cluster D consists of cases where both the mean r and %V(1.5) are extraordinarily large, representing cases with extremely advanced coarsening of nodules. Cluster E is similar to Cluster A in mean r, but it has the largest %V(1.5) and, most uniquely, a value of ρ_θ which is the smallest of the five clusters. In other words, this is a type with incomplete separation of nodules, corresponding to what was designated as quasi-B type in the classification of Miyake (1960), a modification of Nagayo's.

In examining the result of computer-assisted classification, we were struck by the close resemblance of the result to the outline of Gall's classification. It is quite interesting that Gall's classification should be imitated in a trial independently made by a computer. Also, the result is, on the whole, consistent with the classification of Nagayo or that of Miyake. Small discrepancy from their classifications, if present, may be related to the natural history of cirrhosis in Japan: the decrease in the number of Type A and increase in that of Type F (nutritional) during these 40 years.

In any event, it does not seem coincidental that a computer-aided classification should agree so well with the proposals made by prominent pathologists. However, this does not mean at all that any pathologist can attain the same conclusion without fail. Not every pathologist can experience the tremendous number of pictures the

Table 8-2. The mean parameter values of cirrhoses assigned to the five clusters.

Cluster	No. cases	Mean r (μm)	%V1.5	Ds (μm)	ρ_θ
A	20	282.1±61.6	14.2±9.5	134.7±45.6	0.42±0.17
B	15	430.2±75.9	26.5±5.8	228.5±50.8	0.47±0.09
C	20	275.3±71.3	9.0±6.6	307.0±59.4	0.54±0.11
D	9	706.3±145.2	41.8±12.0	318.9±97.7	0.36±0.17
E	6	403.0±75.7	44.8±3.7	146.3±41.6	0.06±0.10

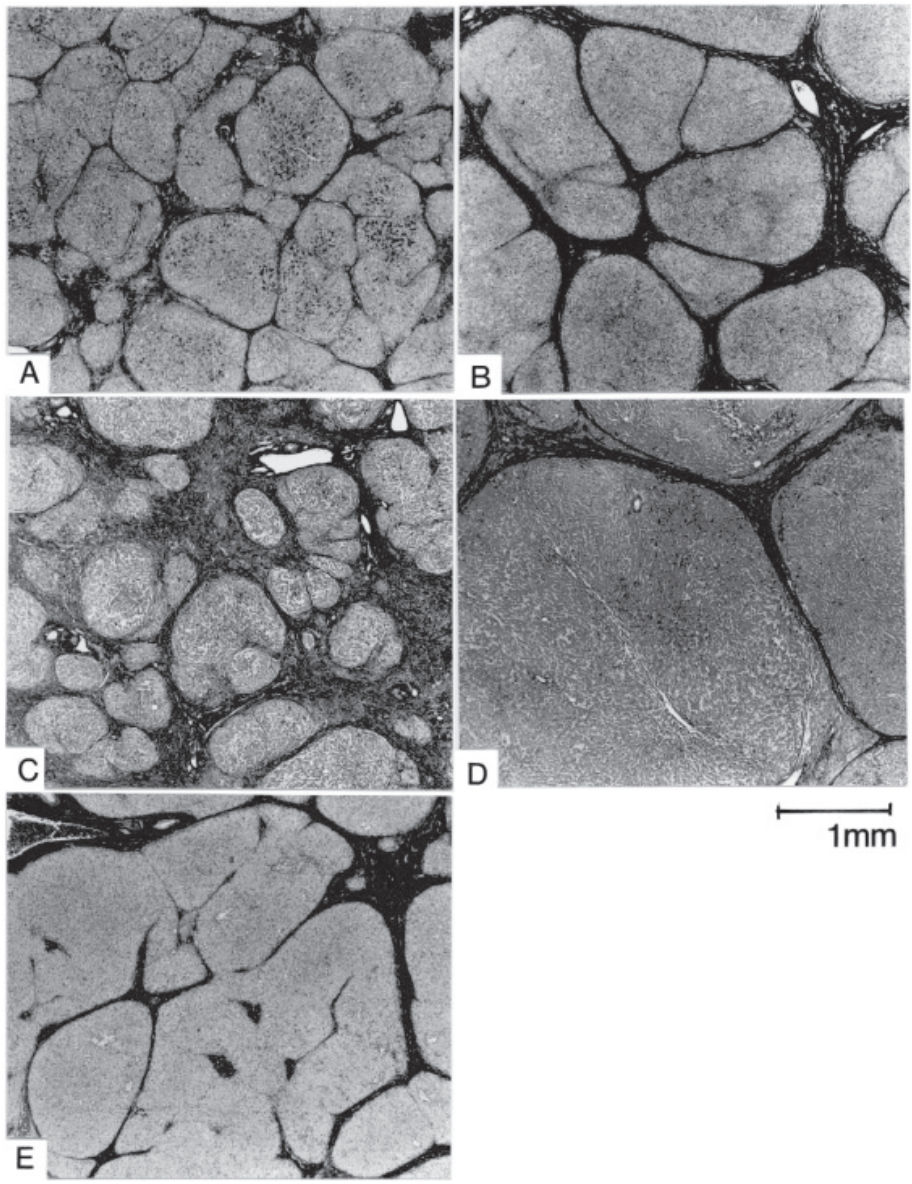

Fig. 8-7. Microscopic pictures of the cases representing the five clusters.

founders of these classifications must have studied. We think therefore, the merit of computerized classification lies in that, the conclusion reached only by a few authorities, is reproducible by common pathologists no matter how much he or she may be experienced in the field.

b) Adequate classification of carcinomatous and precarcinomatous cells

i) Adenocarcinoma of lung and its precursor

Pulmonary adenocarcinoma and AAH (Figs. 8-8, 8-9)

Of the various adenocarcinomas arising from the lung, Clara cell type (Fig. 8-8 upper left) and Type-II pneumocyte-type (Fig. 8-8 upper right) are two major varieties, both in the classification proposed by Shimosato (1989). The former type was coined as such on account of hobnail-shaped carcinoma cells reminiscent of Clara cells. In the latter, the cuboidal shape of cells was considered analogous to Type II pneumocytes which in normal lung secrete surfactant. In the early, pre-invasive stages of development, both types of carcinoma cells grow so as to extend along the surface of alveolar septa, replacing the pre-existing epithelial cells. Recently, attention has been paid to a lung lesion considered to be a forerunner of adenocarcinoma. Called atypical adenomatous hyperplasia, or AAH, the lesion resembles the picture of non-invasive adenocarcinoma but differs from carcinoma in the grade of atypia that appears somewhat lower. Exhibited in the lower part of Fig. 8-8 are two examples of what were diagnosed by our team as AAH before morphometric analysis. However, the degree of atypia is not the same; the lesion in the right seems more atypical, with the atypical nuclei arranged at a higher density than in the left. Its difference from non-invasive

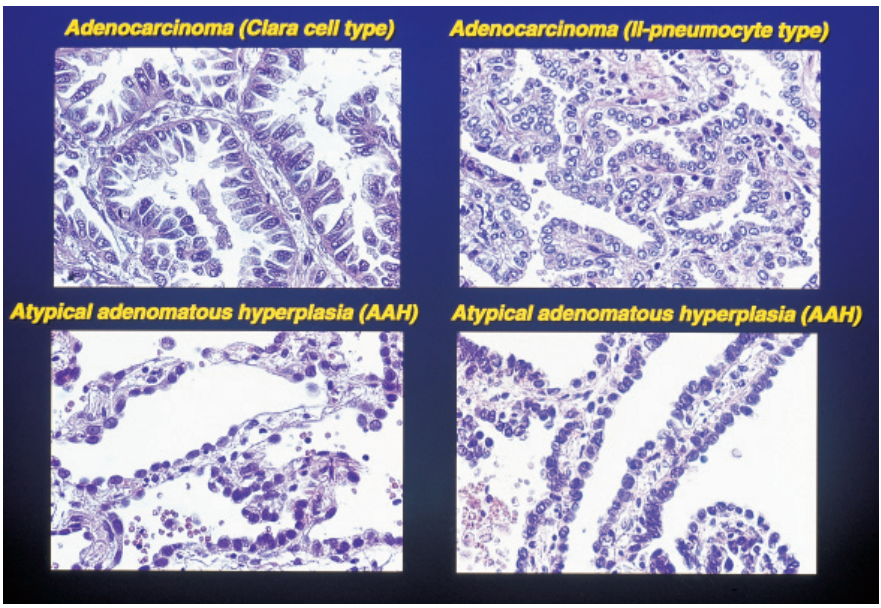

Fig. 8-8. Microphotographs of pulmonary adenocarcinoma and its related lesions. The upper left: adenocarcinoma of Clara cell type. The upper right: adenocarcinoma of Type II pneumocyte type. Both of the pictures in the lower half are from the lesions diagnosed as atypical adenomatous hyperplasia (AAH) before morphometry, where however the cells in the right seem more atypical than those in the left. Hematoxylin and eosin stain.

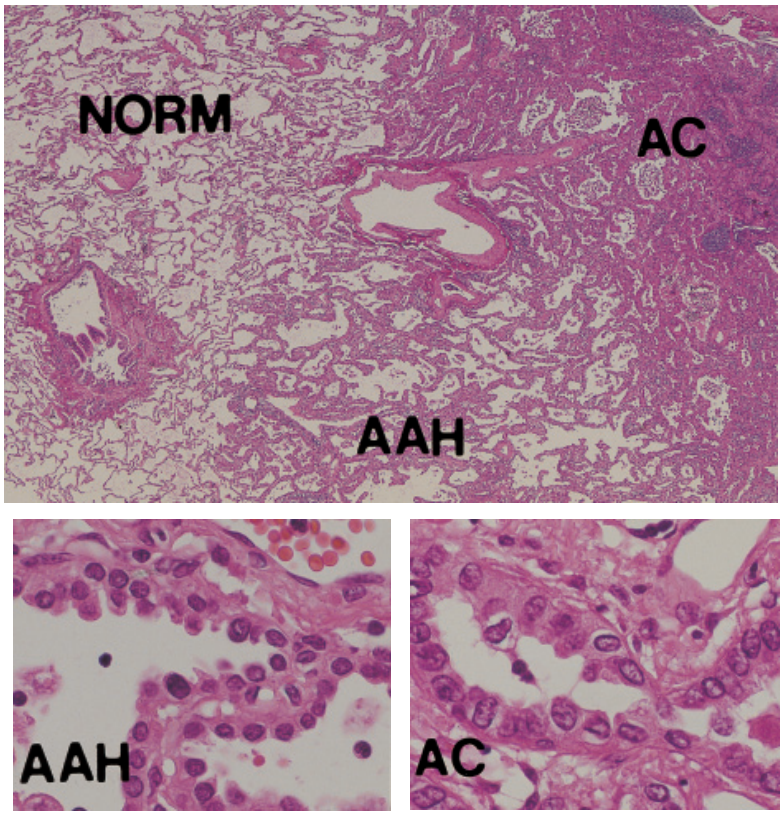

Fig. 8-9. Microscopic picture of an adenocarcinoma of lung (AC), surrounded by a zone of atypical adenomatous hyperplasia (AAH). Hematoxylin and eosin stain.

carcinoma, particularly the Type II pneumocyte-type, seems so delicate as to make us unsure about whether we can reproduce our diagnosis without fail. In view of this, Mori *et al*. (1993, 1996ab) attempted to apply cluster analysis to AAH and the two types of adenocarcinoma.

It is well evidenced that the AAH corresponds to one of the steps preceding the development of adenocarcinoma, both for the Clara cell type and Type-II pneumocyte-type (Nakanishi, 1990). In Fig. 8-9, a zone of AAH is shown surrounding a non-invasive adenocarcinoma, a finding often encountered while examining lungs surgically resected for carcinoma. This reminds us of the concentric zonation of different atypia already shown in the adenoma-carcinoma sequence of colon (Fig. 4-36) and dysplasia-carcinoma sequence of bile ducts (Fig. 4-44).

Parameter expression of cellular atypia (Figs. 8-10, 8-11)

In studying the difference among the adenocarcinomas and AAH by cluster analysis, the feature of atypical cells has to be reduced to several parameters. An atypical cell is recognized as such based on a series of factors constituting its form. In the

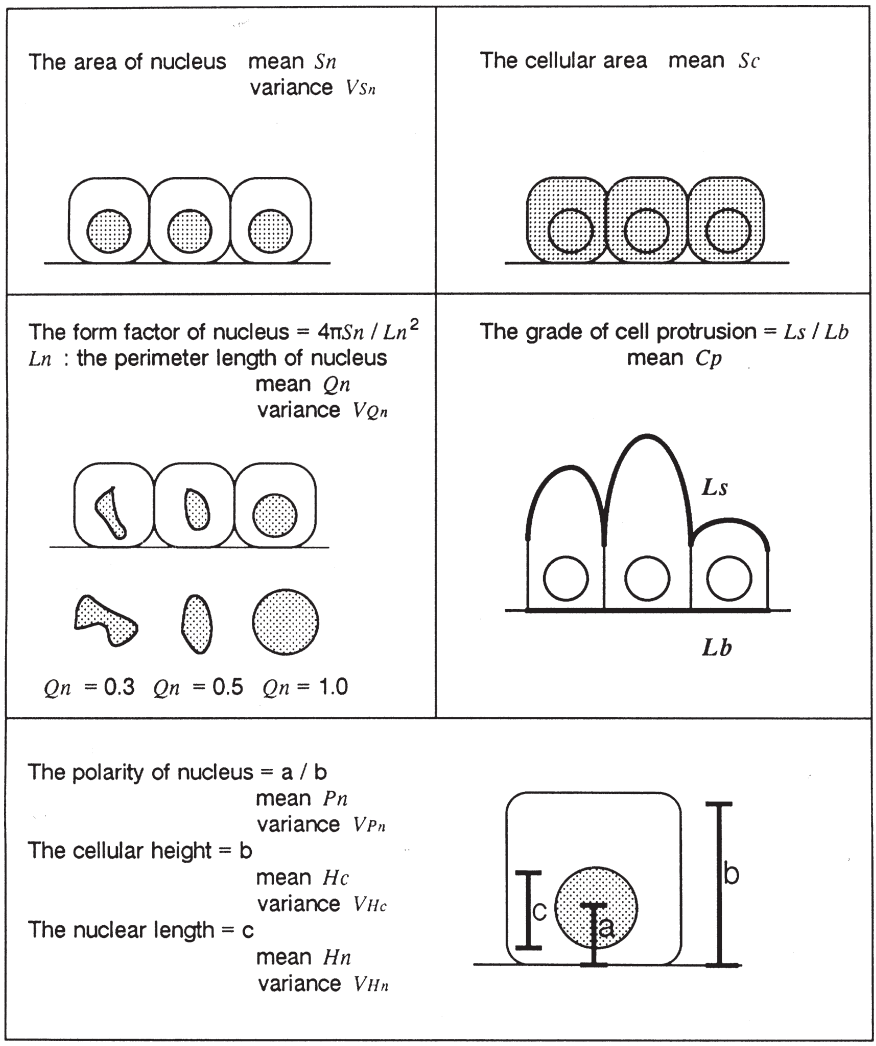

Fig. 8-10. Parameters employed to express the grade of cellular abnormality in quantitative terms. Reproduced from Mori, Takahashi *et al.*: Cancer (1993) 72: pp. 2334.

present study, twelve factors of cell form were taken as atypia-associated, each defined quantitatively as in Fig. 8-10. These include the nuclear area (S_n), the form factor (Q_n) of nucleus and the cellular area (S_c), all with the mean and variance, and the grade of cell protrusion (C_p). To these, the polarity of nucleus (P_n, positioning at the cell base), cellular height and the nuclear length were added as secondary parameters. Of these, the form factor of nucleus (Q_n) is defined as

$$Q_n = 4\pi \cdot S_n/L_n^2 \ (0 \leqq Q_n \leqq 1.0)$$

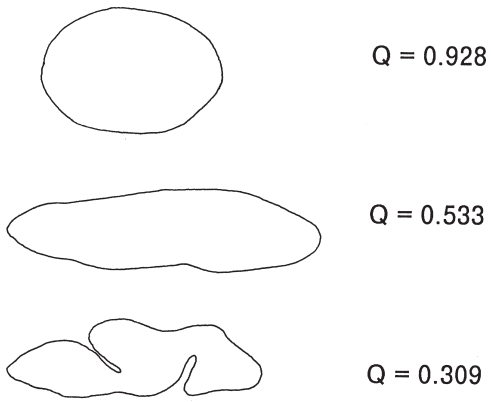

Fig. 8-11. The form factor of nucleus Q_n applied to three examples of closed profiles.

where L_n is the perimeter length of nucleus. As schematized in Fig. 8-11, the value of Q_n is 1.0 when the nucleus is exactly circular. The more elongated or indented the nuclear shape, the smaller does the value become, thus serving as a measure of irregularity in the shape of nucleus. C_p, the grade of cell protrusion was introduced to express the "hobnail" pattern, a rugged contour of apical surface, which characterizes Clara cell type adenocarcinoma with cells having high-positioned nuclei.

The material was a total of 97 lesions selected from surgical lung specimens. Pre-morphometry microscopic diagnosis was: Clara cell type adenocarcinoma in 35 lesions, Type II pneumocyte-type adenocarcinoma in 22, and AAH in 40. In each lesion, b & w microphotographs were taken from ten fields at a magnification of ×1,200 with a Polaroid camera attached to the microscope. The photographs were placed on a digitizer, and the contours of typical lining cells and their nuclei were inputted into a digital image analyzer by tracing with a cursor. About 100 non-fragmented cells with complete nuclear outlines were sampled for each lesion.

Cluster analysis of AAH_S and adenocarcinomas (Figs. 8-12, 8-13)

Figure 8-12 demonstrates the result of cluster analysis for the 97 lesions. Clearly, the lesions proved to be classifiable into three clusters. Entered along the lower margin of the dendrogram are the microscopic diagnoses of the lesions given before morphometry: "C" (yellow) denotes Clara cell type adenocarcinoma, "2" (blue) Type II pneumocyte type adenocarcinoma, and "AAH" (red) aypical adenomatous hyperplasia. It is shown that the lesions diagnosed as Clara cell carcinoma were classified into Cluster 3 without exception. Of the lesions diagnosed as Type II pneumocyte carcinoma, a single lesion each was found astray into Cluster 2 and Cluster 3, but the remaining 20 lesions were all classified into Cluster 1. Thus it may be clear that Cluster 3 is a group of Clara cell type and Cluster 1, that of Type II pneumocyte-type carcinoma.

However, most intriguing was the separation into two groups of the 40 lesions that were given a pre-morphometry diagnosis of AAH: 25 of them were classified into

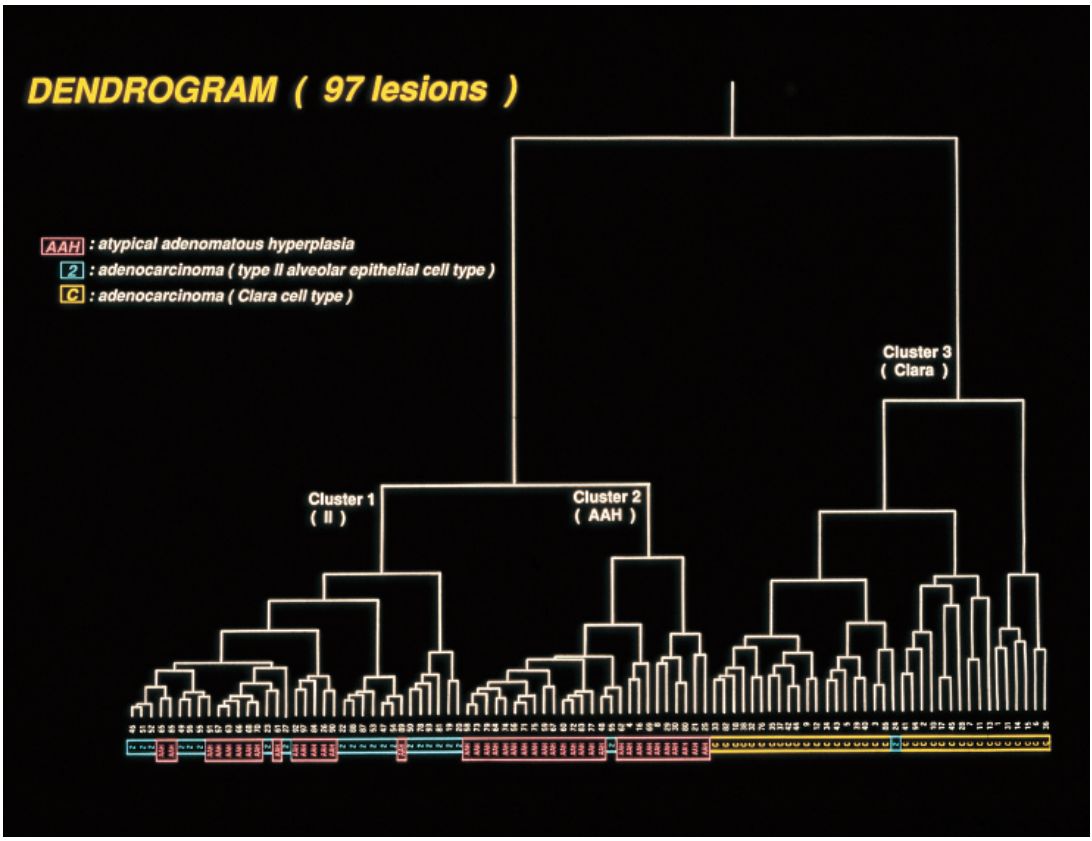

Fig. 8-12. A dendrogram showing the result of cluster analysis for 97 lung tumors. Arranged along the lower margin are the microscopic diagnoses given before morphometry. "C" (yellow): Clara cell type adenocarcinoma. "2" (blue): adenocarcinoma of Type II pneumocyte type. "AAH" (red): atypical adenomatous hyperplasia. The lesions proved to group themselves into three clusters. Of these, Cluster 3 appears to be representing Clara cell type adenocarcinomas and Cluster 1 Type II pneumocyte adenocarcinomas. However, the 40 cases diagnosed as AAH were split into Clusters 1 and 2. Reproduced from Mori, Takahashi *et al*.: Cancer (1993) 72: pp. 2337.

Cluster 2, and 15 into Cluster 1. Allotted to Cluster 2 were 26 lesions, of which as many as 25 were those diagnosed as AAH, with only one additional lesion diagnosed as Type II cell carcinoma. This seems suggesting that Cluster 2 is the very group proper to AAH. While a pre-morphometry diagnosis of AAH was given to the remaining 15 lesions, they were shown forming Cluster 1 together with Type II cell carcinoma. In a re-examination of microscopic pictures after the cluster analysis, it was confirmed that in the 25 lesions grouped into Cluster 2, the form of cells were typical of AAH, while in the 15 lesions classified into Cluster 1, the cell shape may not have been so much like AAH as Type II pneumocyte-type carcinoma.

This seemed to be urging us to reconsider the way we had been making microscopic diagnosis. After this study, our stance changed into such a way as to consider,

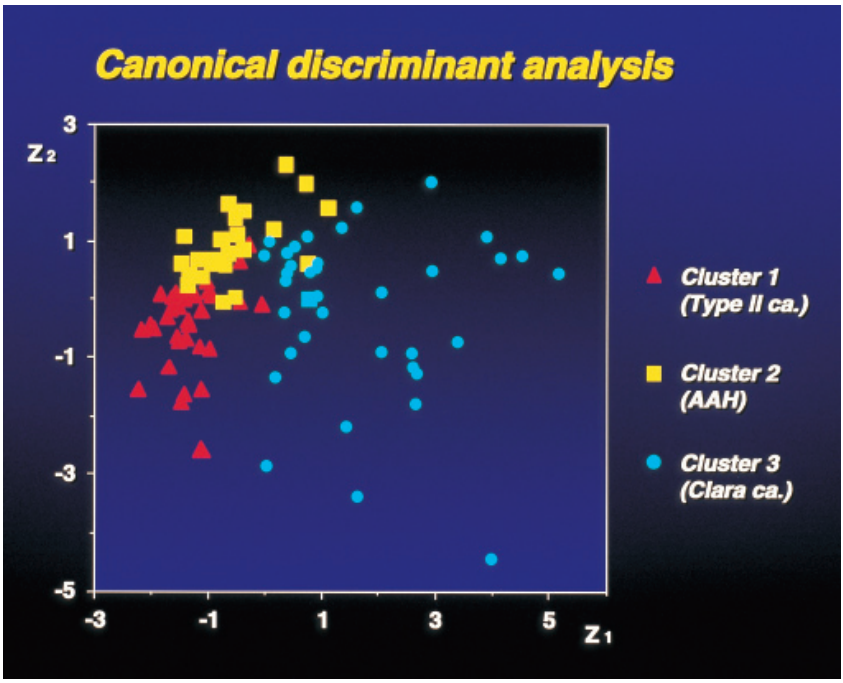

Fig. 8-13. Scattergram showing the result of canonical discriminant analysis for the 97 lesions. z_1, the first, and z_2, the second canonical variate. Note that the cases classified into Cluster 2 (AAH) form a group that is positioned between Clusters 1 and 3, suggesting that in the development of adenocarcinoma, AAH corresponds to a common progenitor. Reproduced from Mori, Takahashi *et al.*: Cancer (1993) 72: pp. 2339.

while examining a lesion like AAH, whether the lesion is to be classified into the group of adenocarcinoma (Cluster 1) or AAH (Cluster 2). When the lesion is evaluated as being high-grade, we think we should not hesitate in making a diagnosis of (Type-II pneumocyte-type) adenocarcinoma.

Figure 8-13 is the result of canonical discriminant analysis, where the result is expressed in a 2-D scattergram. The abscissa (z_1) is the first, and the ordinate (z_2) the second canonical variate. Here the distribution of individual lesions faithfully reflects the result of cluster analysis shown in the dendrogram: the lesions assigned to the three clusters are well separated, but the lesions classified into Cluster 2 (AAH) are, as a whole, positioned between Cluster 1 and Cluster 3. This seems to be suggesting that in the development of adenocarcinoma, AAH corresponds to a common progenitor that has a potential to develop into either type of carcinoma.

ii) Carcinoma and dysplasia of pancreatic duct

Intraductal papillary adenoma of pancreas (Figs. 8-14, 8-15)

Carcinoma of the pancreas is considered to originate from epithelia lining the pancreatic duct in various level of ductal tree. Sometimes, papillary tumor arises in

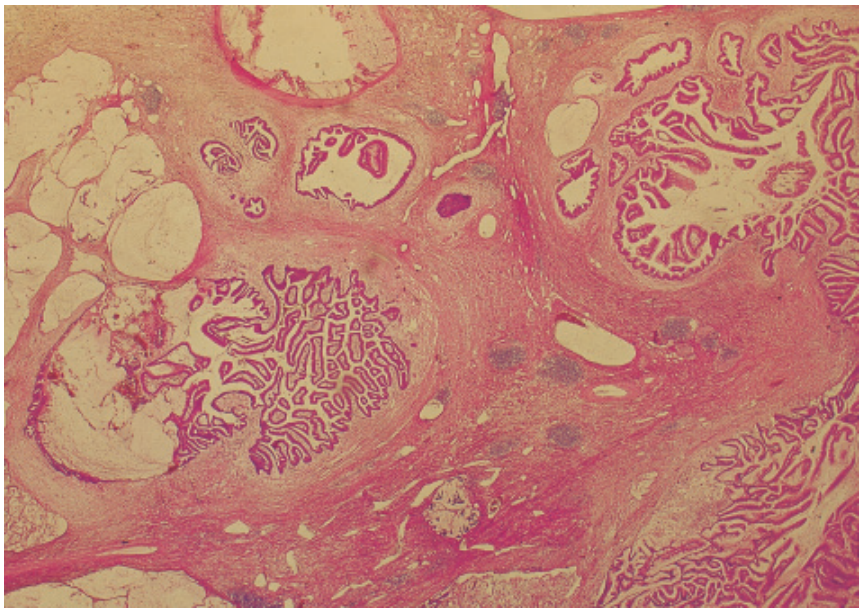

Fig. 8-14. Intraductal papillary adenoma of pancreas. Low power microphotograph. There are multiple cystic lesions, all lined with adenoma cells producing mucinous products into the tubular lumina. Hematoxylin-eosin stain.

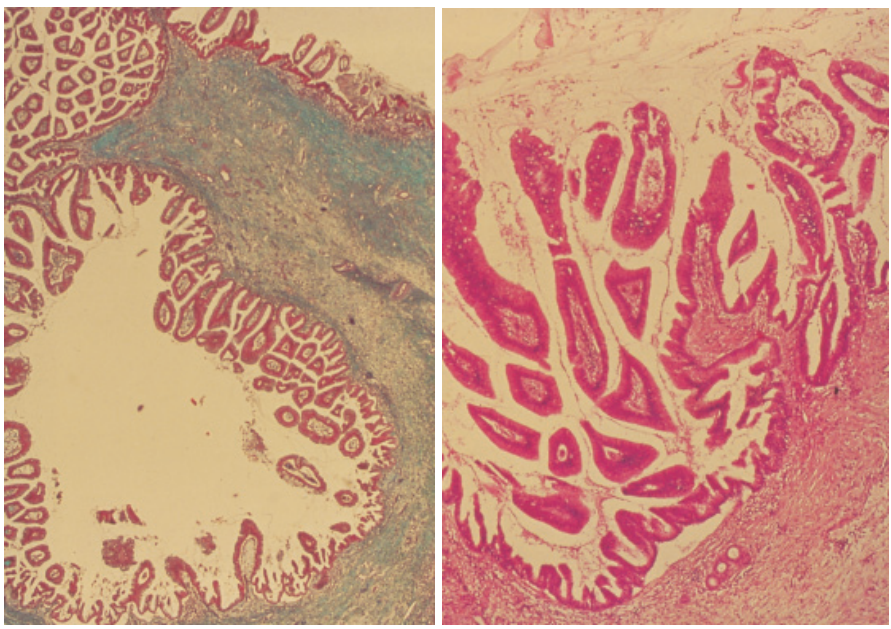

Fig. 8-15. Intraductal papillary adenoma of Fig. 8-14 shown at a higher magnification. The adenoma cells lining the inner surface of the cystic lumina are mildly atypical and with markedly papillary coutour. Elastica-Goldner (left) and hematoxylin-eosin stain (right).

larger pancreatic ducts. Given various expressions as intraductal papillary adenoma, mucus-hypersecreting tumor or cystadenoma, the tumor is regarded as representing one of the multiple steps in the carcinogenesis of pancreatic duct (Klöppel, 1980; Pour *et al*., 1982). As shown in Fig. 8-14, this tumor extends in the ductal tunnels and emerges in a section as multiple intraductal masses.

At a higher magnification, papillary growth of the lining cells is prominent (Fig. 8-15). In this picture the cells look moderately atypical, but among the cases, the grade of atypia is variable. Also within a case, pictures with different grades of atypia ranging from mild nuclear atypia to overt carcinoma *in situ* (CIS), can co-exist forming a mosaic of mucosal patches. Here we are likely to have a situation similar to the development of adenocarcinoma in adenoma of the large bowel, hepatohilar bile duct carcinoma and pulmonary adenocarcinoma. In view of this, Furukawa *et al*. (1992) performed a 3-D mapping of various grades of atypia in 12 surgical specimens of pancreas with this tumor.

Grade of cell atypia (Fig. 8-16)

Figure 8-16 presents examples of lining cells with various grades of atypia, each diagnosed before morphometry and cluster analysis. In the left upper part one can see ordinary epithelia of pancreatic duct. In the right upper, hyperplastic cells are shown with papillary projections and single row of slightly enlarged nuclei. Demonstrated in the left lower was diagnosed as dysplasia with moderately atypical nuclei arranged along the basal side but in slight disorder. The right lower was considered to be CIS with marked irregularity in nuclear size and shape and loss of polarity.

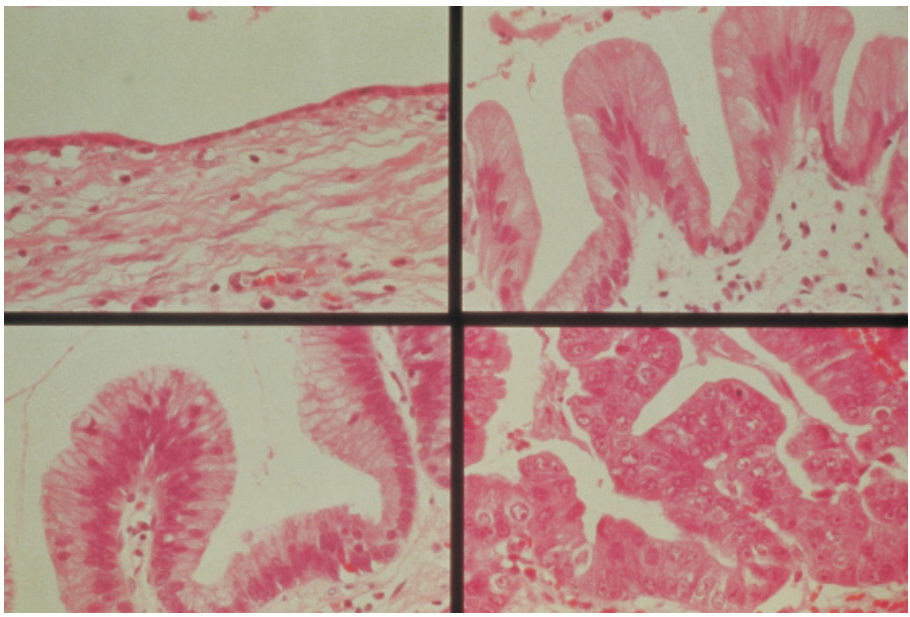

Fig. 8-16. Various grades of atypia found in the adenoma cells. Hematoxylin-eosin stain.

3-D mapping of intraductal tumors using "macroserials" (Figs. 8-17, 8-18)

Figure 8-17 demonstrates a surgical specimen of pancreas harboring intraductal papillary adenoma, which was "gelatin embedded" and reduced to "macroserials" using a ham slicer, in the same way as we applied to the slicing of livers (Chapter 4; Fig. 4-42). All the slices were re-embeded in paraffin, and their sectional pictures were subjected to 3-D reconstruction.

Figure 8-18 demonstrates the result of 3-D mapping in a case of intraductal papillary tumor. The main pancreatic duct and several primary subbranches dividing from

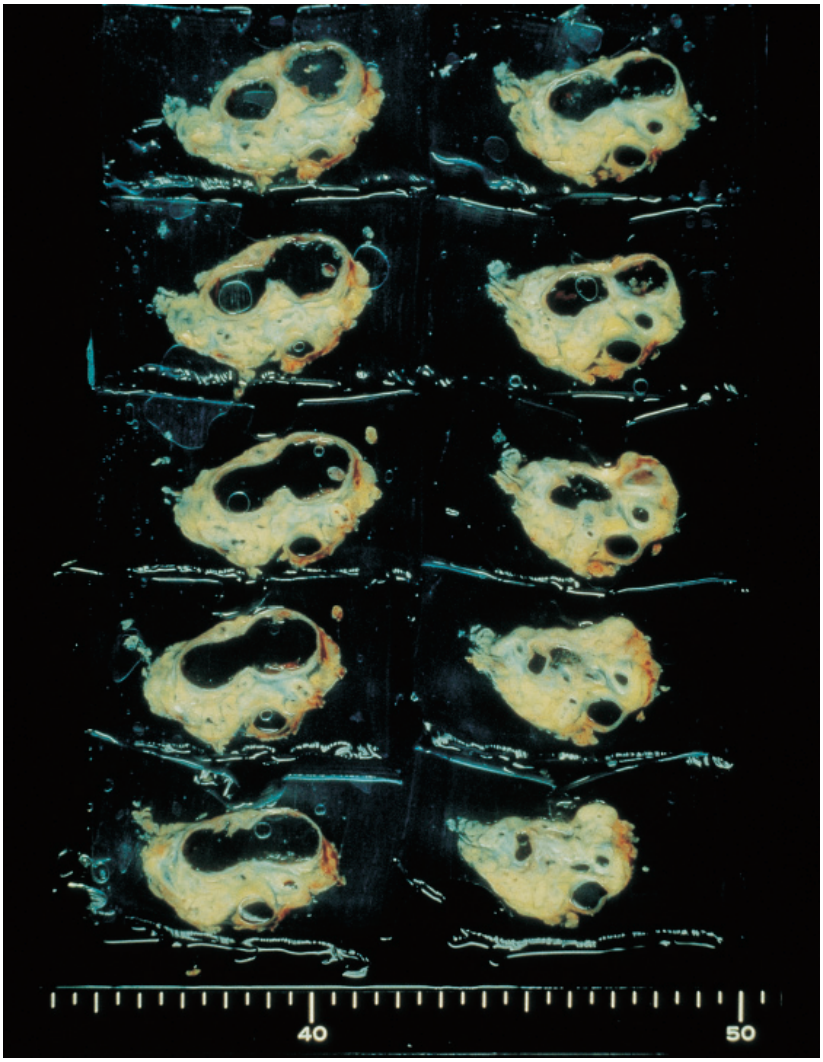

Fig. 8-17. "Macroserials" of surgically excised pancreas harboring intraductal papillary adenoma. The pancreas was embedded in gelatin and serially sliced with a ham slicer. Reproduced from Furukawa, Takahashi *et al*.: Cancer (1992) 70: pp. 1507.

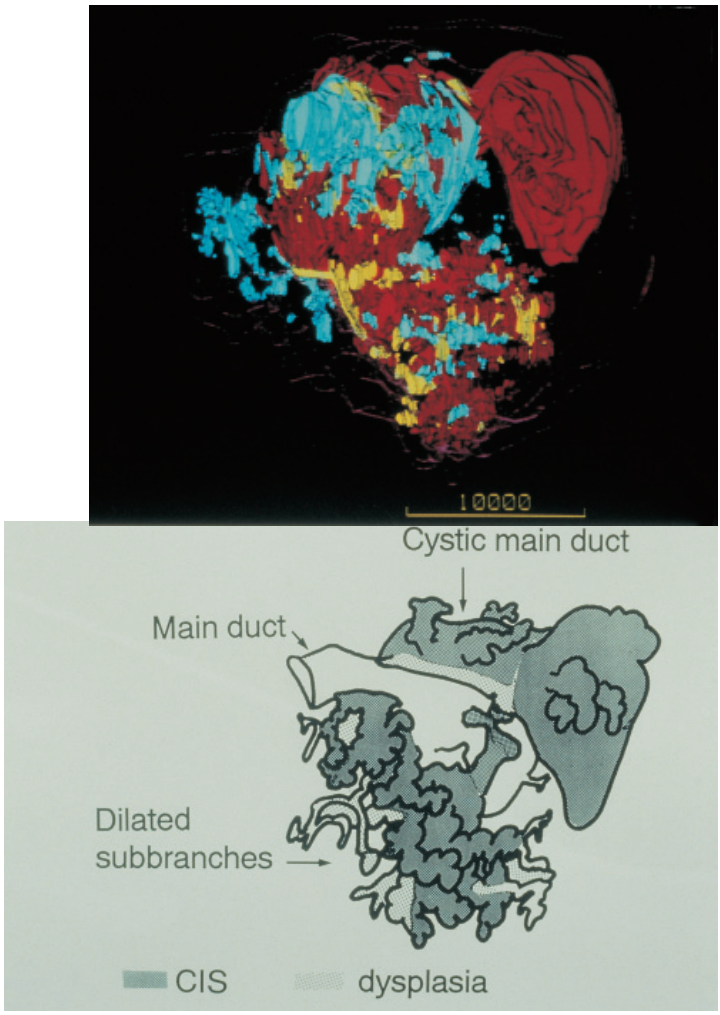

Fig. 8-18. Computer-assisted 3-D mapping of intraductal papillary adenoma in the pancreatic ducts. The main duct is dilated focally in the upper right part, corresponding to a major cyst, which is lined with non-invasive carcinoma cells (CIS) as painted in red. Painted in light blue are areas with normal duct epithelia. Around the CIS, small patchy areas having dysplasia are dispersed (yellow). Reproduced from Furukawa, Takahashi *et al*.: Cancer (1992) 70: pp. 1507.

the main duct are strongly dilated due to intraductal growth of tumor. Of the ectatic ducts, those painted in red contain CIS, those yellow are ducts lined by dysplastic cells, and light blue are ducts having ordinary lining cells. Although the arrangement of the three areas seems complicated and intertwisted, it seems at least that around the areas of carcinoma are zones of dysplasia, justifying also here to assume progression of multistep carcinogenesis.

Cluster analysis for atypical ductal cells of pancreas (Fig. 8-19)

Based on the above, Furukawa attempted at applying cluster analysis to atypical cells lining the pancreatic ducts (1994). The form of atypical cells was reduced to a combination of nine parameters, all defined in basically the same way as in lung adenocarcinomas. The material included microscopic sections of pancreas from 53 patients subjected to partial or total pancreatectomy. The pathological diagnosis of the pancreatic disease was adenocarcinoma, intraductal papillary adenoma, chronic or acute pancreatitis. Of the 53 pancreases, a total of 78 areas with ductal epithelia were selected for morphometry, with some of the pancreases harboring within-case variation in the grades of atypia. The 78 areas were so sampled as to cover the whole range of changes from ordinary epithelia to hyperplastic epithelia to dysplasia to cells with severe atypia consistent with a diagnosis of CIS, and to invasive adenocarcinoma. A sampled area was divided into five parts, from each of which a microphotograph was taken at a high-power magnification of ×1,200 so that more than 150 nuclei may be included for each of the sample areas. The microphotographs were placed on a digitizer, and the cellular as well as nuclear contours were inputted into a computer by tracing with a cursor.

Exhibited in Fig. 8-19 is the result of cluster analysis in the form of dendrogram.

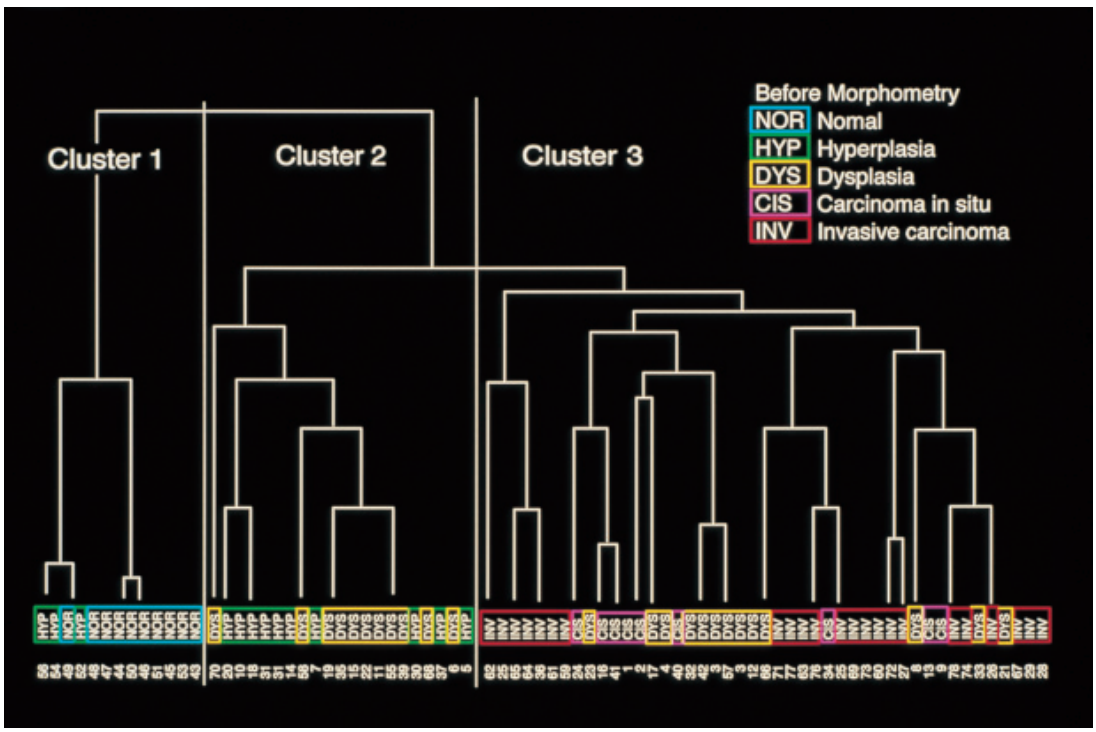

Fig. 8-19. A dendrogram showing the result of cluster analysis of pancreatic duct cells from the 78 lesions with epithelial atypia. Note the clear separation into Clusters 1, 2 and 3. NOR indicates ordinary epithelia; HYP, lesion diagnosed as hyperplasia; DYS, dysplasia; CIS, carcinoma in situ; INV, invasive carcinoma. Reproduced from Furukawa, Takahashi *et al*.: Arch Pathol Lab Med (1994) 118: pp. 230.

The numbers arranged along the lower margin are those of the samples, and arranged upon these are the diagnoses given before morphometry to each of the samples: NOR, normal epithelia; HYP, hyperplastic cells; DYS, dysplasia; CIS, carcinoma in situ; INV, invasive carcinoma. As shown, the 78 samples were separated into three clusters. Cluster 1, comprising 10 areas diagnosed as having normal cells and 3 with hyperplastic cells, was definable as the cluster of ordinary cells. On the other hand, all the areas, to which a pre-morphometry diagnosis of invasive or in situ carcinoma was given, were classified into Cluster 3 without exception. Accordingly, this cluster may well be definable as a cluster of carcinoma. Twenty areas were assigned to Cluster 2, with 9 of them having a diagnosis of hyperplasia and the remaining 11 that of dysplasia, suggesting that this is a cluster of benign lesion with mild atypia. However, there were another 13 samples diagnosed as having displasia but classified into Cluster 3, the cluster of carcinoma. Thus, here again, it has been shown that the lesions that seemed to be dysplasia before morophometry were, in reality, not a single category, but contained heterogeneous groups of atypical cells. Cluster analysis made it clear that they have to be separated further into mild and severe dysplasias, the latter being indistinguishable from carcinoma in terms of cellular morphology. For us, this study was a lesson, and according to what was shown, we have changed our standard of microscopic diagnosis.

Analysis of *ki-ras* mutation related with clusters (Fig. 8-20, Table 8-3)

After cluster analysis was performed, some of the samples were selected for PCR and dot blot analysis of mutations at codon 12 of *ki-ras*.

Fifty of the 78 samples were subjected to analysis (Table 8-3). The remaining 28 samples were omitted because of limited amount of cells available and/or, of inadequate state of samples in terms of fixation. In this study, the 50 samples were divided according to the result of cluster analysis, ordinary cells (Cluster 1), cells with mild dysplasia (benign atypical lesions; Cluster 2) and cells with severe dysplasia (malignant atypical lesions; Cluster 3). It was shown that in Cluster 3 including severe dysplasia and carcinoma, as many as 86% of samples were harboring mutation, while even in Cluster 2 which was thought to comprise only cells with benign lesions, the mutation proved to exist in 82%, a ratio comparable to the cluster of carcinoma.

Data like this may be found in many reports, but the point is that in the present study, DNA analysis was performed for atypical cells that were classified in a *reproducible* way. Usually in this sort of DNA analysis, pathologists are asked to determine, on inspection basis, whether the studied cells are dysplasia or carcinoma.

Table 8-3. The result of *ki-ras* analysis for atypical cells subjected to classification by cluster-analysis.

Morphology	Number of samples	Mutations
Ordinary cells (Cluster 1)	11	0
Mild dysplasia (Cluster 2)	17	14 (82%)
Severe dysplasia (Cluster 3)	22	19 (86%)

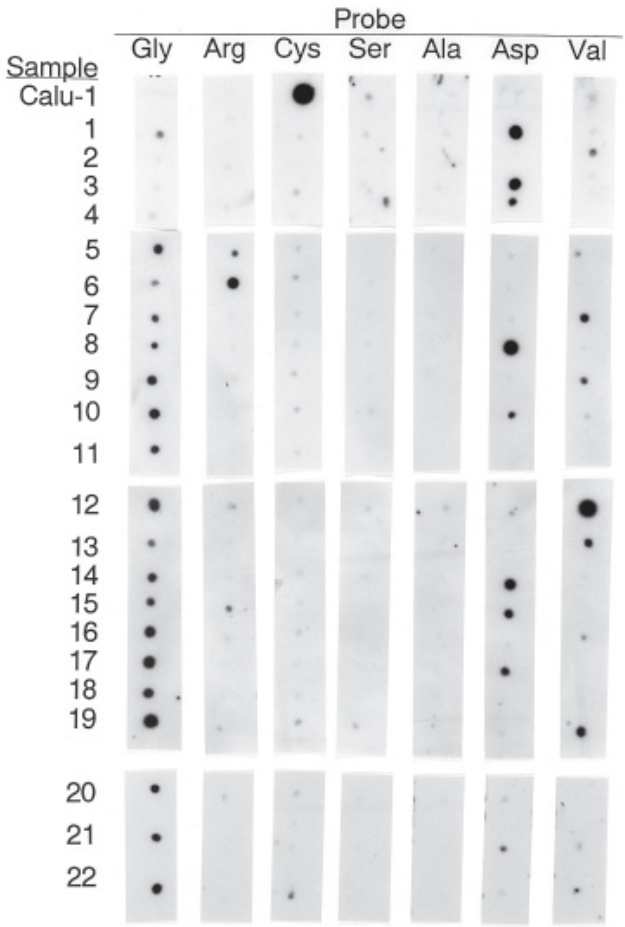

Fig. 8-20. Dot-blot analysis for point mutation at codon 12 of *ki-ras* using the materials classified by cluster analysis shown in Fig. 8-19.

If reproducibility is not ensured in the microscopic differentiation of atypical cells, a firm reliable basis cannot be provided for the DNA analysis either.

On closing this chapter, it should be added that in our team, cluster analysis found application to still other studies. Of such studies, small comment is to be given to that of Tezuka *et al*. and M. Nakamura *et al*.

In a series of studies dealing with endometrial carcinoma and related lesions, Tezuka *et al*. (1994) subjected the cell pattern of smear preparations to 5-variate cluster analysis. The material was aspirated samples from 70 cases. In 10 of the cases the diagnosis before morphometry was well differentiated adenocarcinomas and in 4 cases, endometrial hyperplasia. Besides, there were 56 normal controls. Cellular pictures from the 70 cases proved to separate squarely into three clusters: Cluster C including

10 cases of adenocarcinoma and 2 cases of atypical hyperplasia, Cluster B including 39 normal cases and 2 cases of adenomatous hyperplasia, and Cluster A including 17 cases which were all histopathologically normal. Thus, the study indicated that morphometric-statistical classification could be of great help in improving the cytodiagnostic validity and reproducibility of endometrial carcinoma.

M. Nakamura *et al*. (1996) attempted to re-examine the histological classification of hepatocellular carcinoma based on cluster analysis. To the parameters of atypia they added a quantity corresponding to the mean breadth (D) of cell nests and thus expressing structural abnormality. Cluster analysis resulted in the separation of the sampled 47 cases into Clusters 1, 2a and 2b, with the picture increasingly atypical in this order. The difference of D-value among the cases proved to be most contributing to the separation of clusters. On DNA ploidy analysis which was performed on the same samples, aneuploid and tetraploid nuclei were shown to increase in the above order, suggesting that this may also be reflecting the growing order of malignancy.